NAVAL POSTGRADUATE SCHOOL

MONTEREY, CALIFORNIA

DISSERTATION

FINE SURFACE CONTROL OF FLEXIBLE SPACE MIRRORS USING ADAPTIVE OPTICS AND ROBUST CONTROL

by

Daniel C. Burtz

March 2009

Dissertation Supervisor: Brij N. Agrawal

Approved for public release, distribution is unlimited.

THIS PAGE INTENTIONALLY LEFT BLANK

REPORT DOCUMENTATION PAGE			Form Approved OMB No. 0704-0188
Public reporting burden for this collection of information is estimated to average 1 hour per response, including the time for reviewing instruction, searching existing data sources, gathering and maintaining the data needed, and completing and reviewing the collection of information. Send comments regarding this burden estimate or any other aspect of this collection of information, including suggestions for reducing this burden, to Washington headquarters Services, Directorate for Information Operations and Reports, 1215 Jefferson Davis Highway, Suite 1204, Arlington, VA 22202-4302, and to the Office of Management and Budget, Paperwork Reduction Project (0704-0188) Washington DC 20503.			
1. AGENCY USE ONLY ***(Leave blank)***	**2. REPORT DATE** March 2009	**3. REPORT TYPE AND DATES COVERED** Dissertation	
4. TITLE AND SUBTITLE: Fine Surface Control of Flexible Space Mirrors Using Adaptive Optics and Robust Control		**5. FUNDING NUMBERS**	
6. AUTHOR(S) Daniel C. Burtz			
7. PERFORMING ORGANIZATION NAME(S) AND ADDRESS(ES) Naval Postgraduate School Monterey, CA 93943-5000		**8. PERFORMING ORGANIZATION REPORT NUMBER**	
9. SPONSORING / MONITORING AGENCY NAME(S) AND ADDRESS(ES) N/A		**10. SPONSORING / MONITORING AGENCY REPORT NUMBER**	
11. SUPPLEMENTARY NOTES The views expressed in this thesis are those of the author and do not reflect the official policy or position of the Department of Defense or the U.S. Government.			
12a. DISTRIBUTION / AVAILABILITY STATEMENT Approved for public release; distribution is unlimited		**12b. DISTRIBUTION CODE**	

13. ABSTRACT (maximum 200 words)

Future space telescopes will contain lightweight, flexible, segmented mirrors. Traditional control approaches for mirror alignment and shape control may be inadequate due to flexibilities and low natural frequencies. Using adaptive optics for space telescopes presents a possible solution. This research proposes innovative H_∞ robust control techniques for these types of systems. An H_∞ controller is synthesized for a complex analytical model with 997 inputs, 936 outputs, and 332 states. To accomplish this, a new technique for model reduction using Zernike polynomials was developed. The H_∞ controller was able to achieve a minimum 15 Hz control bandwidth. The previous integral controller was unable to meet the 10 Hz bandwidth requirement. The H_∞ design process used was validated on a simpler adaptive optics testbed. The experimental verification also showed that the robust control techniques outperformed the classical control techniques in the presence of disturbances.

The significant contributions are a Zernike polynomial method for model reduction, robust controller synthesis for a complex adaptive optics analytical model, and experimental verification on an AO testbed. Although the robust control design is more complex, it provides improved performance in the presence of uncertainty in the disturbances and modeling.

14. SUBJECT TERMS Robust control, adaptive optics, segmented mirrors, Shack-Hartmann wavefront sensor, space telescopes, H_∞, flexible structures	**15. NUMBER OF PAGES** 115
	16. PRICE CODE

17. SECURITY CLASSIFICATION OF REPORT	**18. SECURITY CLASSIFICATION OF THIS PAGE**	**19. SECURITY CLASSIFICATION OF ABSTRACT**	**20. LIMITATION OF ABSTRACT**
Unclassified	Unclassified	Unclassified	UU

NSN 7540-01-280-5500 Standard Form 298 (Rev. 2-89)
Prescribed by ANSI Std. 239-18

THIS PAGE INTENTIONALLY LEFT BLANK

Approved for public release; distribution is unlimited

FINE SURFACE CONTROL OF FLEXIBLE SPACE MIRRORS USING ADAPTIVE OPTICS AND ROBUST CONTROL

Daniel C. Burtz
Major, United States Air Force
B.S., United States Air Force Academy, 1997
M.Eng., University of Colorado, 1998

Submitted in partial fulfillment of the
requirements for the degree of

DOCTOR OF PHILOSOPHY IN ASTRONAUTICAL ENGINEERING

from the

NAVAL POSTGRADUATE SCHOOL
March 2009

Author: _____
Daniel C. Burtz

Approved by:

_____
Brij N. Agrawal
Distinguished Professor of Mechanical and Astronautical Engineering
Dissertation Supervisor and Committee Chair

_____
Marcello Romano
Assistant Professor of Mechanical and Astronautical Engineering

_____
Oleg Yakimenko
Associate Professor of Mechanical and Astronautical Engineering

_____
Roberto Cristi
Professor of Electrical and Computer Engineering

_____
Ty Martinez
Naval Research Laboratory

Approved by: _____
Knox Millsaps, Chair, Department of Mechanical and Astronautical Engineering

Approved by: _____
Douglas Moses, Associate Provost for Academic Affairs

THIS PAGE INTENTIONALLY LEFT BLANK

ABSTRACT

Future space telescopes will contain lightweight, flexible, segmented mirrors. Traditional control approaches for mirror alignment and shape control may be inadequate due to flexibilities and low natural frequencies. Using adaptive optics for space telescopes presents a possible solution. This research proposes innovative H_∞ robust control techniques for these types of systems. An H_∞ controller is synthesized for a complex analytical model with 997 inputs, 936 outputs, and 332 states. To accomplish this, a new technique for model reduction using Zernike polynomials was developed. The H_∞ controller was able to achieve a minimum 15 Hz control bandwidth. The previous integral controller was unable to meet the 10 Hz bandwidth requirement. The H_∞ design process used was validated on a simpler adaptive optics testbed. The experimental verification also showed that the robust control techniques outperformed the classical control techniques in the presence of disturbances.

The significant contributions are a Zernike polynomial method for model reduction, robust controller synthesis for a complex adaptive optics analytical model, and experimental verification on an AO testbed. Although the robust control design is more complex, it provides improved performance in the presence of uncertainty in the disturbances and modeling.

THIS PAGE INTENTIONALLY LEFT BLANK

TABLE OF CONTENTS

LIST OF FIGURES

LIST OF TABLES

THIS PAGE INTENTIONALLY LEFT BLANK

ACKNOWLEDGMENTS

I would like to thank the members of my committee for their encouragement and guidance in preparing this dissertation. They have devoted numerous hours to instructing me, and providing constructive comments to improve my final product. I also owe a special debt of gratitude to my fellow researchers in the Spacecraft Research and Design Center, Professor Jae Jun Kim, Dr. Hyungjoo Yoon, and Dr. Anne Marie Johnson. Despite having their own work to do, they were always willing to stop what they were doing to help me solve a problem or understand a concept more clearly. Their assistance was invaluable.

Special thanks also goes to Dr. Alain Carrier and his colleagues for their insights into the analytical segmented space telescope model. His availability to answer my questions and provide suggestions for areas needing further research was quite helpful.

Dr. Sergio Restaino and Dr. Ty Martinez from the Naval Research Lab were instrumental in the setup and operation of the testbed hardware. Capt Matt Allen, USAF, did much of the initial development work on the testbed algorithms.

Finally, I am extremely grateful to my wife Angie, partly for her efforts in helping to edit my dissertation, but mostly for helping keep me sane during this process and shouldering the majority of the work of raising two small boys while I conducted my research.

THIS PAGE INTENTIONALLY LEFT BLANK

I. INTRODUCTION

A. MOTIVATION

Optical systems have long been used for imagery and intelligence gathering for both civilian and military purposes. Since the first recorded use of telescopes in the early 17th century, the goal has been to improve the technology that would give the user the advantage of increased resolution at greater distance. Some of the early pioneers in the field such as Galileo and Newton experimented with refractive (lens) and reflective (mirror) systems. As the technologies allowing remote optical sensing evolved, military commanders on the battlefield, as well as naval commanders at sea, found new applications for them. Naturally, the military application of these tactics evolved with the advent of air and space vehicles from which to conduct reconnaissance. The trend has continually moved towards smaller angular resolution at increased distance.

As shown in Equation (1.1), the diffraction limited angular resolution using Raleigh criterion, as denoted by α_R, is a function of the wavelength of the electromagnetic radiation, approximately 600 nanometers for visible light, and the diameter, *D*, of the light gathering aperture

$$\alpha_R = 1.22\lambda / D \tag{1.1}$$

The angular diffraction limited resolution is usually measured in radians, arcseconds, or some equivalent measure. Since the wavelength being observed is usually fixed, the aperture diameter is the only remaining variable factor. Obviously, there are physical size limitations to which the primary optic in a telescope can be manufactured.

The most obvious limitation arises from the physical process of machining the lens or mirror. Ideally, a reflective mirror would have a parabolic shape to minimize the amount of aberration resulting from the reflection process. In practice, however, spherical mirrors are much easier to machine, giving rise to one of the most common optical aberrations, appropriately known as spherical. Additional constraints on the diameter of the primary optic arise in the support structure used to encase or hold the optic stationary. Large telescope optics will often be quite rigid, a design characteristic to

prevent sagging or warping of the optical surface due to gravitational or other inertial forces. Mechanisms to support and move these heavy optics can themselves become quite large and cumbersome.

This support structure problem has less consequence for ground-based observing platforms, but for airborne platforms, weight becomes more important. This realization becomes immensely important when considering space-based platforms where the cost per pound to orbit is prohibitively high. Space platforms are perhaps even more limited by size constraints than weight constraints. The basic shape of every launch vehicle that launches spacecraft into orbit is cylindrical. Even the space shuttle orbiter, whose exterior is *not* cylindrical, has a cylindrical payload bay that carries the spacecraft aloft. The diameter of the rocket body becomes a physical limitation for the size of the primary optic of a space-based telescope. Considering the distance involved in orbital altitudes, this diameter is certainly less than that needed to achieve the angular resolution desired by image analysts.

Despite these challenges, the attraction of space-based imagery, and in particular, high altitude imagery, is quite appealing. Beyond the immediate advantages of a wider field of view and higher vantage point, a high altitude orbit also results in lower orbital speeds, which translates to increased dwell time over a given part of the earth. This can be taken to the extreme of the geostationary orbit, which would maintain continual presence over a point above the equator and have nearly a third of the surface of the planet in its field of view at any time. The tradeoff comes in the distance to geostationary altitude. Whereas a low earth orbiting satellite might orbit a few hundred kilometers above the surface, geostationary spacecraft require an altitude of approximately 36,000 km. The effect of this distance is illustrated in Figure 1 and Equation (1.2), where the angular resolution is equal to that from Equation (1.1), and R represents, in this case, distance from the orbital altitude to the surface of the earth.

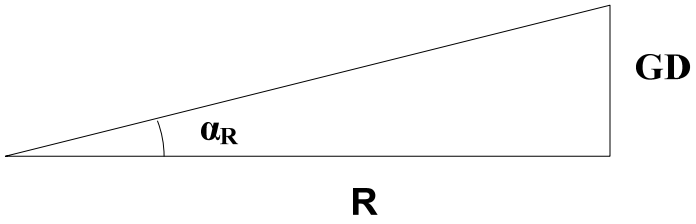

Figure 1 Angular Resolution Geometry.

$$R\alpha_R = GD \tag{1.2}$$

where *GD* is the ground resolution.

Although increasing altitude does not decrease the angular resolution per se, it does increase the minimum separation needed to differentiate two objects on the surface. Said another way, space telescopes at geostationary altitudes require much larger diameter primary optics to differentiate the same level of ground detail as low earth orbiting satellites. Clearly, a way is needed to combine the benefits of better image quality obtained from lower orbits with that of improved dwell time from higher orbits. Multiple solutions exist and are not limited to individual spacecraft. A concept of operations could be developed which utilizes a constellation of spacecraft at varying altitudes to maximize resolution and dwell time over particular areas of interest. Another solution involves achieving primary optic diameters larger than would fit inside a conventional payload fairing, by segmenting, and deploying on orbit. These segmentation techniques will be the topic of this dissertation.

Traditional telescopes utilize a spherical, continuous face sheet mirror. Its size is constrained, however, by the aforementioned limitations. If instead of a continuous face sheet, the primary optic can be made of a series of smaller segments, these segments can be folded or packaged in some way that the segments are deployed or assembled into a large diameter mirror after the rocket's payload fairings have been jettisoned and the spacecraft is on-orbit. The concept is not unlike that which is done with spacecraft solar arrays, which are often folded like an accordion before launch and unfolded once in

space. To be clear, though, the on-orbit assembly of mirror segments is vastly more complex than that of solar arrays, communications antennas, or any other spacecraft structures deployed on-orbit.

The added complexity stems partly from the fact that mirror segments are extremely delicate components with sensitive optical coatings, but primarily from the precise alignment criteria required of the segments. Recall that the wavelength of visible light is on the order of 600 nm. With wavelengths this small, even a slight misalignment of mirror segments can cause aberrations to degrade image quality beyond what is useful. This problem is so daunting in fact, that a separate area of research is being devoted entirely to the problem of initial alignment for segmented optics [1]. Once the coarse initial alignment has been successfully accomplished, only fine adjustments will be necessary to account for remaining optical aberrations. More on those aberrations will be discussed later. This research will focus only on the finer surface corrections after initial alignment has been completed.

Numerous folding and deploying scenarios could be considered for segmented optics. One important design criterion is the electromagnetic radiation wavelength collected through the aperture. The emphasis here will be on visible wavelengths. A current example of a space telescope under construction that will utilize segmented optics is NASA's James Webb Space Telescope, an infrared astronomy telescope planned for launch in 2013. An artist's concept of this spacecraft is shown in Figure 2. Notice the gold-colored primary optic, which is comprised of 18 hexagonal segments. The launch configuration of this spacecraft calls for the three leftmost and three rightmost segments to be folded back in order to fit within the payload fairings. Two hinged motions will deploy those six segments along with a host of other deployments from the launch configuration involving, but not limited to, the struts supporting the secondary optic and the blue and red sun shield. Although the primary optic deployment may seem rather simple, it is important to remember that the remaining twelve segments are still individual segments, and vibrations and stresses of the launch environment will make for a very challenging initial alignment problem.

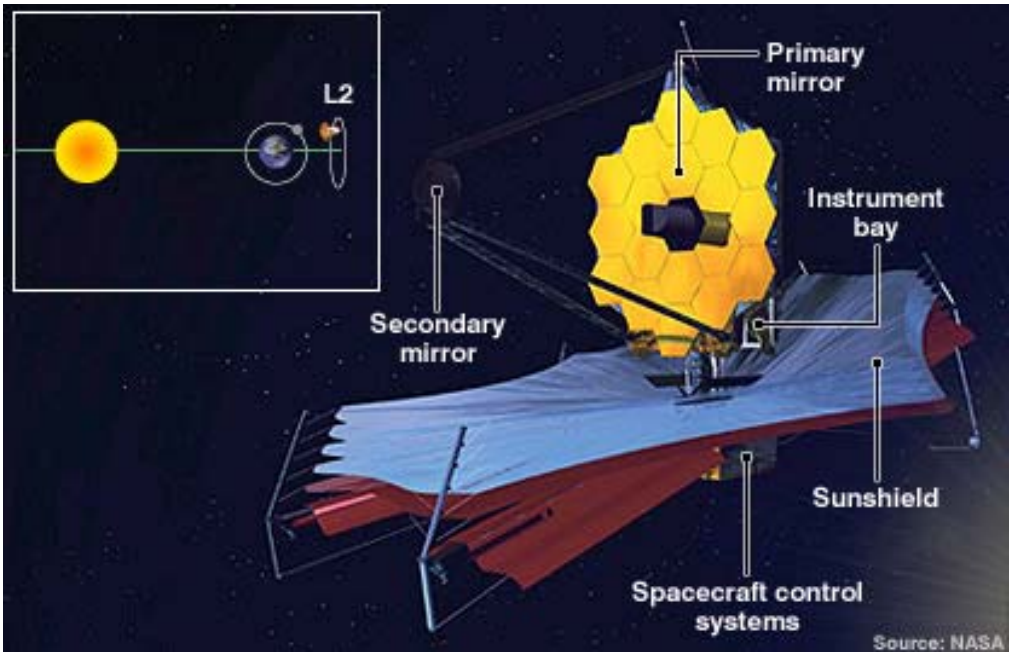

Figure 2 James Webb Space Telescope From [2].

Another challenging aspect of the space telescope observation platform involves the structural properties of the primary optic. Spacecraft designers are constantly attempting to decrease the mass of the onboard components to reduce the costs of placing them into orbit. Large, rigid, monolithic optics work fine for most terrestrial applications, but their weight becomes prohibitive for spacecraft operations. Whether segmented or a continuous face sheet, space telescope optics are most economical when lightweight. Being lightweight causes particular challenges in the control and alignment of mirror segments or other means of mirror shape control. The natural frequencies will be lower, resulting in control and structure interactions.

Both segmented and continuous face sheet mirrors will have actuators attempting to correct the mirror shape due to measured aberrations. If the bandwidth controlling these actuators overlaps, or even falls close to the natural frequencies of the structure, then the controller may actually exacerbate the aberrations. Typically, large ground-based mirrors have their lowest natural frequency well over 1000 Hz so control bandwidths below 100 Hz have no chance of exciting natural frequencies. With segmented mirrors, such as the one researched in this dissertation, the lowest natural

frequency can be around 30 Hz, which becomes a concern for the control system designer. Additionally, for space platforms, the natural frequencies are often tightly packed and have very little damping. The robust control techniques researched demonstrate an innovative way to design controllers for these lightweight segmented space telescopes.

B. ADAPTIVE OPTICS SYSTEMS

The term adaptive optics refers to any optical system in which some optical component; be it a mirror, lens, or some other device, undergoes adaptation or modification to improve the resulting wavefront. The preceding discussion on controlling the shape of the primary optic on space telescopes fits the general description of an adaptive optics (AO) system. To be clear on the nomenclature, the *adaptive optic* is that component of the system such as the mirror, which is altered; whereas *adaptive optics* usually refers to the entire system.

The optical wavefront is a perpendicular cross section or slice of a propagating beam of photons, which is measured by a wavefront sensing device such as a camera. For example, a beam of coherent light from a laser propagates along a cylindrical path. At that point, taking a sensor measurement at any location or at any instant of time yields a representation of the wavefront. Ideally, the wavefront from a high-quality laser would be planar, or flat. In reality, aberrations cause the wavefront to be non-planar and wavy.

Aberrations in optical systems come from a variety of sources. Light traveling through the vacuum of space would be the most un-aberrated light possible. As the light propagates though a dynamic atmosphere, or any other medium, it becomes aberrated to an observer on the other side of that medium. Other aberrations arise from imperfections in optical components. Even the human eye is not immune to aberrations, hence the need for corrective lenses or eye surgery. For machined optics, the imperfections result from uneven coatings, imperfect shapes, or impurities in glass among others. Light passing

through even one optical component has become aberrated beyond its original form. A moving or vibrating platform can also lead to wavefront aberrations, which is of particular concern for spacecraft.

AO systems come in a variety of styles and designs, but there are usually three components common to all. Those components are a wavefront sensor, an adaptive optical component, and a control computer. This is not unlike a standard control system that consists of a sensor, control algorithm, and actuators influencing a plant. Each of these portions will be discussed subsequently. A generalized schematic is shown in Figure 3. This research focuses exclusively on the design of new and innovative control algorithms. The optical components and wavefront sensors used on the experimental testbed are commercially available, off-the-shelf pieces of hardware. Although the emphasis here is on controls, adaptive optics is truly a multi-disciplinary field and draws on expertise in physics, structures, controls engineering, and electrical engineering to name a few.

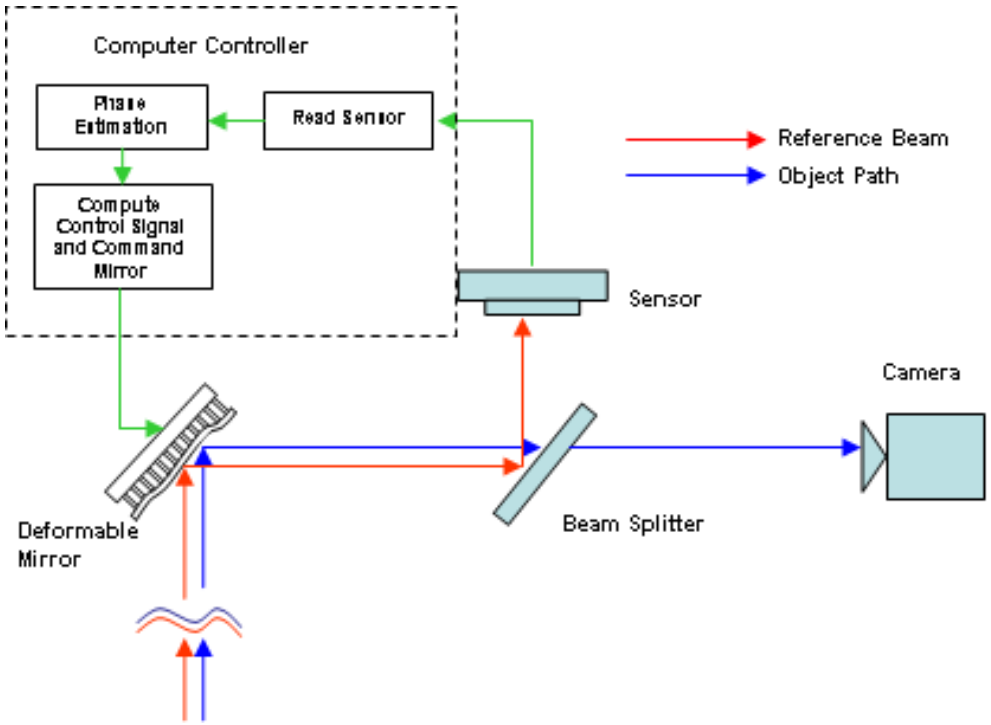

Figure 3 Generalized AO System From [3].

1. Wavefront Sensors

A wavefront sensor takes an optical measurement of some object of interest and represents that information as a set of discrete data points. One of the most common wavefront sensors for AO systems is the Shack-Hartmann wavefront sensor. It consists of two basic parts, a camera, and a lenslet array. The camera operates like any CCD or CMOS camera. Incident light excites pixels in an array and the light intensity is converted to voltages, which is output along with the location of pixels that were excited. The other main element of the Shack-Hartmann wavefront sensor is the lenslet array at the front entrance pupil of the camera. To understand its purpose, first envision a card that is placed at the entrance pupil, blocking all light from reaching the camera sensor. Now poke a series of holes in the card in a geometric pattern, such as a square matrix. Light from the incident wavefront will pass through these holes, undergo diffraction, and strike the CCD sensor. Now replace the holes with an equal number of small lenses (known as lenslets) which abut up against each other such that there is no remaining surface of the card. The entire blockage now consists of a grid of lenslets.

Each of these lenslets is identical and will focus the incoming light on the CCD behind it. The distance from the lenslet array to the CCD is the focal length of the lenslets. For a planar incoming wavefront, the location of the focused spots on the CCD will be evenly spaced in the same geometric pattern as the lenslet array.

If, however, the incoming wavefront is not planar, then the resulting spots on the CCD will not be evenly spaced. Whereas a planar wavefront will come to focus directly behind each lenslet, an aberrated wavefront will cause the spot to come to focus at some x and y displacement on the CCD. Figure 4 shows an example of an x displacement from an aberrated wavefront; a y displacement would be normal to the surface of the page.

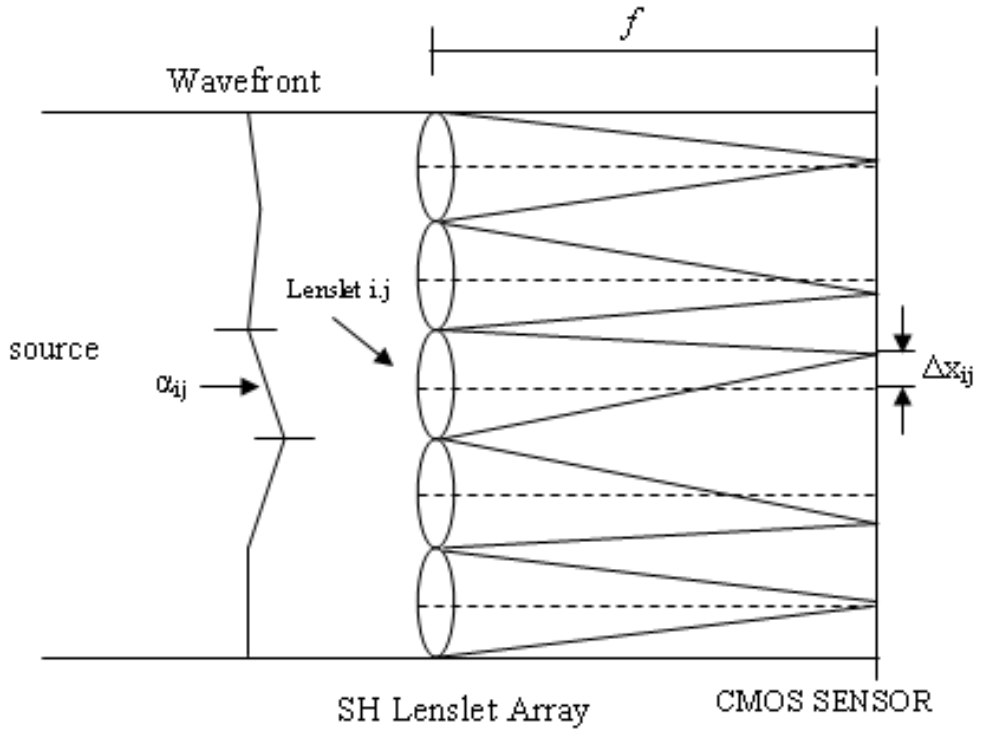

Figure 4 Lenslet Array Spot Formation From [3].

By measuring the actual location of the spots vs. the expected location for a planar wavefront, an estimate of the true shape of the incoming wavefront can be obtained. This information is then used by the control computer to determine what action must be taken to correct the aberration.

The Shack-Hartmann is only one example of a wavefront sensor for an AO system. A phase diversity sensor is another common wavefront sensor that attempts to determine wavefront shape based on the difference in image intensity from typically two cameras placed at different locations in the beam path [4]. Both the analytical model and experimental testbed described in this research use Shack-Hartmann wavefront sensors.

2. Adaptive Optical Components

Once the actual shape of the wavefront has been determined, the control algorithms are needed to determine how best to make the wavefront as planar as possible. First, however, it is best to understand the actual methods available to apply a correction

to the wavefront. This is accomplished through use of an adaptive optic. Perhaps the simplest type of adaptive optic to start with would be a Fast Steering Mirror (FSM). The reflecting surface of an FSM is a normal flat mirror. The difference is in the mounting mechanism that supports the mirror in the system. Imagine a pair of orthogonal axes along the surface of the mirror. These axes are commonly referred to as tip and tilt axes. By making small rotations about these axes, the beam of light the mirror is reflecting can be steered. This ability to alter the orientation of the mirror, and therefore the beam path, allows an FSM to be classified as an adaptive optic and an optical system containing an FSM is likewise classified an AO system. An FSM, however, corrects only first order wave aberrations.

One common source of such aberrations in an optical beam is jitter caused by structural vibrations. Since these vibrations are somewhat oscillatory in nature, if the wavefront sensor is fast enough to identify their frequency, an FSM should be able to apply an appropriate phase difference to null out the jitter aberrations in the optical beam. In this example, the system's actuators affect a change in the FSM's tip/tilt orientation.

For higher order wave aberrations, a more complex adaptive optic such as a deformable mirror is used. Unlike the FSM, which has a continuous, flat, face sheet surface, the surface of a deformable mirror can be adjusted to take on other desired shapes that are *not* flat. This is accomplished with a set of actuators on the back surface of the mirror. Piezoelectric actuators are one type and can be bonded to the back surface such that the actuator can be lengthened or shortened to "push" and "pull" the surface of the mirror into the desired shape. Another type consists of electrostatic actuators where a voltage potential creates a deformation of the mirror surface instead of the motion of a physically attached rod.

The purpose behind deformable mirrors is to create a mirror shape that exactly matches the inverse of the measured wavefront. Therefore, if the wavefront is determined to have a particular shape, then by inverting that shape and applying it to the mirror, the wavefront can be made planar. The success of this approach will depend on several factors including having enough lenslets in the wavefront sensor to accurately characterize the wavefront, a control algorithm capable of quickly determining a solution

before the wavefront changes, and enough actuators to create the inverse wavefront with high enough fidelity. Technology has increased to the point where a large number of lenslets and actuators can be packed into a relatively small space on their respective components. This is advantageous in that it allows higher fidelity shapes to be measured and created. The disadvantage lies in the next topic of discussion, the control laws governing the process.

These two brief descriptions of adaptive optical components only scratch the surface of the level of complexity that can exist in AO systems. Remember that for high altitude space based telescopes, the optics will most likely need to be segmented to provide the degree of resolution required. A telescope comprised of even just two segments presents a significant challenge for the design engineer. Future telescopes will be comprised of several individual segments requiring precise alignment, where each segment is its own deformable mirror requiring face sheet control. The analytical model studied in this research is just such a system.

3. Control Algorithms

Adding lenslets and actuators to an AO system not only increases complexity but also lends itself to coupling between actuators. Whereas historically, control laws treated AO systems as a static problem, and to date, adaptive optics has been a field of study largely belonging to the field of astronomy where AO systems are used to correct for ground based observatories peering at distant starlight through a turbulent atmosphere. Using either a naturally occurring or artificially created guide star, the control computer can determine the atmospheric aberration in the guide star's wavefront and use that information to compensate for the atmosphere with the optics. This can be done in either a real-time or in a post-processing manner. For real-time correction, the computer has to compute and apply the corrections before the atmosphere above the telescope changes. This process is made much simpler by the telescope mirrors being large rigid structures where the control bandwidths are well below the natural frequencies, so the structural dynamics can be ignored in the control design. For lightweight space based telescopes, besides having to contend with natural frequency concerns, there is increased probability

that a large piston motion by a particular actuator will have an unintended effect on the mirror surface in the neighboring actuator's space. This effect is magnified in light of the fact that on current deformable mirrors, large numbers of actuators are packed into relatively small areas. If simply ignored, this coupling will have an adverse effect on system performance. The structural flexibility also cannot be ignored in the control design.

Since the design of robust control algorithms for AO systems is the purpose of this research, this brief introduction for AO control algorithms will be sufficient for now. For a more thorough treatment of AO systems, the reader is referenced to [5], considered a primary resource in the field. Specifics of the exact challenges faced and the solutions to those challenges will be addressed throughout the remainder of this dissertation.

C. OBJECTIVES

1. Analytical

The analytical research has the following objectives:

1. Apply robust control techniques for fine surface control of a complex flexible space mirror to minimize wavefront aberrations.
2. Develop improved model reduction techniques with the emphasis of minimizing wavefront aberration.
3. Achieve the desirable control bandwidth.

2. Experimental

The experimental research has the following objectives:

1. Apply robust control to an adaptive optics testbed.
2. Compare the performance of robust control and currently used classical control techniques.

D. CURRENT STATE OF RESEARCH IN THE FIELD

Although the majority of AO system controllers have been of a classical nature, there has been some initial research into advanced robust control techniques for AO systems. To date, the author is not aware of any operational systems that employ a robust controller based on H_∞ techniques. The work of Frazier et al. has looked at incorporating some of these techniques onto testbed systems [6], [7], [8], [9]. Their work has been done on simple testbed setups quite similar to the Spacecraft Research and Design Center adaptive optics testbed at the Naval Postgraduate School used in this research. The adaptive optic in their research was also a 37 channel deformable mirror.

Kun Li et al. have investigated H_∞ control techniques for segmented telescopes [10], but their approach involves using centralized, decentralized, and overlapping control architectures to handle the complexity of large numbers of states, inputs, and outputs. The technique presented here will instead focus on model reduction techniques to synthesize the H_∞ controller. Other works have begun to apply H_∞ techniques to large ground based telescopes that have more flexibility than previous generation telescopes, similar to what space based telescopes will experience [11], [12], [13].

The general theory of H_∞ control techniques is much more developed than the application to AO systems. Several papers and textbooks have been written that have advanced these techniques on benchmark problems [14], [15], [16], [17]. These works have not been specific to segmented space telescope applications, however. This research will adapt these techniques for complex space telescope models.

The most thorough work on H_∞ control techniques for lightweight segmented optics has been done by Carrier [18]. His research looked at modeling and robust control techniques for the Advanced Structure/Control Integrated Experiment (ASCIE) testbed, a segmented optical system also used by [10]. In physical appearance, the ASCIE is quite similar to the space telescope model used in this research. It contains hexagonal mirror segments for the primary optic and a lightweight truss support structure. Unlike the model used for this dissertation, however, the ASCIE is not an adaptive optics system. It

contains only 24 sensor inputs versus the 936 sensor measurements used here, and only 18 actuators versus the 997 used here. Also because of some of the computational limitations at the time, the control design was broken into subsystems. Processor capabilities have matured enough to negate the need to form separate subsystems; however, a model reduction is still required. Nonetheless, the modeling and advanced control techniques developed by Carrier form the foundation for much of the application in this dissertation.

Specifically, the work on the ASCIE demonstrated that stochastic controller design methods were impractical due to sensitivities to unmodeled dynamics, modal frequency uncertainty, and modal damping uncertainty. Worst case, or H_∞, methods yielded a 10% stability margin to modal frequency uncertainties. Furthermore, the research developed the technique of using input and output multiplicative uncertainties for loopshaping purposes.

This research will take the foundational work from these sources and adapt it for use on a significantly more complex segmented space telescope model. Specifically, the techniques will be adapted for AO systems and the requirement to perform model reduction prior to controller synthesis. The robust controller synthesis process used will be experimentally validated on an AO testbed. A testbed for the analytical model was not available, however, so the control techniques will be demonstrated on a simpler setup and suite of equipment.

E. DISSERTATION OUTLINE

Chapter II of this dissertation will give detailed descriptions of the complex space telescope model along with the AO testbed and its components. Chapter III will give an overview of robust control and the factors considered in the design of robust controllers. Chapter IV will describe the model reduction techniques necessary for the synthesis of the robust controller. Chapter V will apply the model reduction and robust controller synthesis theory to the analytical model and show the performance when subjected to an input disturbance. Chapter VI will describe the same process for the experimental results on the AO testbed. Final analysis and conclusions will be given in Chapter VII.

F. CONTRIBUTIONS

The present research has contributed to the state-of-the-art in the following areas:

1. An H_∞ robust control technique has been used for surface control of a flexible space telescope model including structural dynamics.
2. Robust control techniques have been able to provide a desired control bandwidth that was not possible with classical control.
3. A new model reduction technique using Zernike polynomials and singular value decomposition has been developed. This technique has been found to provide better performance to reduce the wavefront aberration in the space telescope model.
4. A robust control technique has been applied experimentally to the adaptive optics testbed of the Naval Postgraduate School Spacecraft Research and Design Center. The robust control technique has been found to be superior to classical control in response time and disturbance rejection.

THIS PAGE INTENTIONALLY LEFT BLANK

II. TESTBED AND MODEL OVERVIEW

A. SEGMENTED SPACE TELESCOPE MODEL

1. Model Purpose

The analytical model researched in this dissertation is a state space model for a space telescope with a segmented primary optic. It was developed and provided by an industry partner as part of a government program to test viability and technology readiness for future space-based telescopes. The model represents an actual system built for test purposes, but not as a flight test model. It involves the latest state-of-the-art technologies for space telescope systems. The analytical research conducted in this dissertation does not involve the actual hardware, only the simulation model.

The model is restricted to the optical payload, and does not include the supporting spacecraft bus. At a basic level it is not unlike other space telescopes with a Cassegrain configuration in that it has a primary mirror that reflects the incoming light back to a secondary mirror, which in turn reflects the light back through a hole in the center of the primary mirror. A suite of science and calibration sensors is located behind the primary optic. The James Webb Space Telescope shown in Figure 2 also has this basic configuration.

Due to the nature of government contracts and funding, this program was somewhat constrained in scope. For example, the control system used standard classical control methods with notch filters. The nature of the system, however, lends itself to research into the feasibility of robust controllers. This is just one of several examples of additional research that could be accomplished on this model.

2. Model Complexity

The segmented space telescope model is extremely complex. It contains 332 states, 997 inputs, and 936 outputs. This is the main reason that model reduction is necessary before a robust controller can be synthesized. The 332 states come from 166 modes identified in a Finite Element Analysis. The inputs correspond to actuators for

mirror surface control and the outputs are sensor measurements. Most, but not all, of the sensor measurements are of the wavefront. By means of comparison, the segmented space telescope model investigated in [10], which is actually quite similar in appearance and function to the model investigated in this research, has 70 states, 18 inputs, and 18 outputs. The Giant Segmented Mirror Telescope in [12] has 200 states and 91 inputs. The AO testbed in [7] has 37 inputs and 162 outputs. The benchmark problems in [14] and [15] typically have on the order of 10 states. Therefore, as can be seen, the scope and complexity of this model is much greater than that of previous studies.

For this model, the primary mirror is comprised of six identical hexagonal segments. They are arranged in a circular pattern such that in the center is another similarly sized hexagon, only vacant, allowing the light reflected off the secondary optic to pass through to the science instruments. The positioning of the individual segments is accomplished by six coarse control actuators and three fine control actuators per segment, for a total of 54 positioning actuator inputs. Each segment also has a grid of 156 face sheet actuators, for a total of 936 shape control inputs, making each segment a deformable mirror. Besides the adaptive primary optic, this model also has another adaptive optic, a Fast Steering Mirror (FSM), located in the vicinity of the science instruments, and is used to remove global tip and tilt jitter motions. There are an additional seven inputs related to the operation of the FSM thus accounting for the 997 total model inputs.

The model outputs similarly come from several different sources. The majority come from a Shack-Hartmann wavefront sensor. Each of the six segments has 61 Shack-Hartmann lenslets associated with it. Each of these lenslets provides two output measurements, an x slope, and a y slope. This results in 732 total Shack-Hartmann outputs. Figure 5 shows a diagram of all six hexagonal segments and the individual lenslets associated with each segment. The lenslets are numbered for one of the segments, which will be important for later discussion. The other segments are numbered sequentially in a counter-clockwise wise direction and the individual lenslets in each segment are numbered similarly if each segment is rotated to the top position.

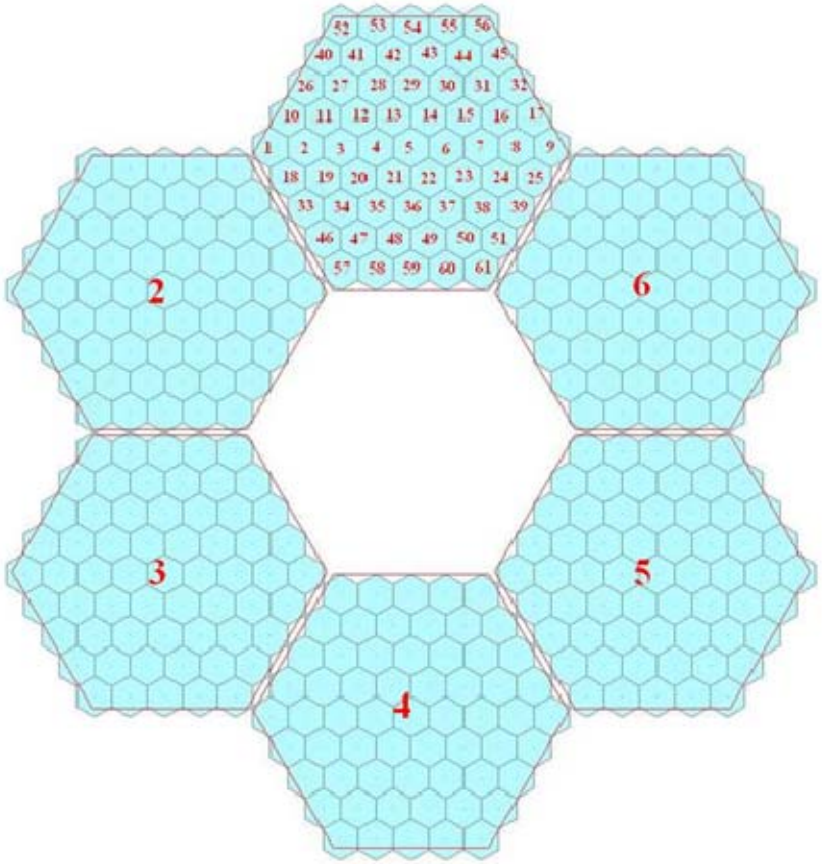

Figure 5 Mirror Segment and Lenslet Orientation.

The model also has a phase diversity wavefront sensor providing 1 piston, 1 tip, and 1 tilt measurement per segment for 18 total, and a jitter sensor providing 2 total tip/tilt measurements. The remaining sensors on the model are 18 gap sensors, three per segment, which measure the distance separating adjacent segments. In sum, there are 770 total sensor measurements. The remaining 166 outputs are the position states. Table 1 provides a summary of the model inputs and outputs.

Inputs

Source	Number	per segment
Face Sheet Actuators	936	156
Fine Control Actuators	18	3
Coarse Control Actuators	36	6
Fast Steering Mirror Actuators	7	
Total	**997**	

Outputs

Source	Number	per segment
Shack-Hartmann Slopes	732	122
Phase Diversity Sensor	18	3
Gap Sensor	18	3
Jitter Sensor	2	
Position States	166	
Total	**932**	

Table 1 Segmented Space Telescope Input/Output Summary.

B. ADAPTIVE OPTICS TESTBED

1. Layout

The Spacecraft Research and Design Center (SRDC) at the Naval Postgraduate School (NPS) has a high quality adaptive optics testbed, which was developed in conjunction with personnel from the Naval Research Laboratory (NRL) in Albuquerque, NM. The purpose of the testbed is to apply control techniques to remove aberrations from an optical wavefront. One application that demonstrates this purpose is an imagery application, where adaptive optics are used to improve the image quality of an object of interest. Figure 6 and Figure 7 show an example of the improvement in image quality that can be obtained using this technique. The four lights at the bottom are LEDs used to illuminate the object.

Figure 6 Uncorrected AO Testbed Image.

Figure 7 Corrected AO Testbed Image.

The primary components of the testbed include two deformable mirrors and two Shack-Hartmann wavefront sensors, two fast steering mirrors, a reference laser, a source object, and a science camera. The reference and object light beams are conveyed around

the table by several lenses, mirrors, and beam splitters which relay the pupil plane to the different components. A schematic of the testbed is shown in Figure 8 and a picture is shown in Figure 9.

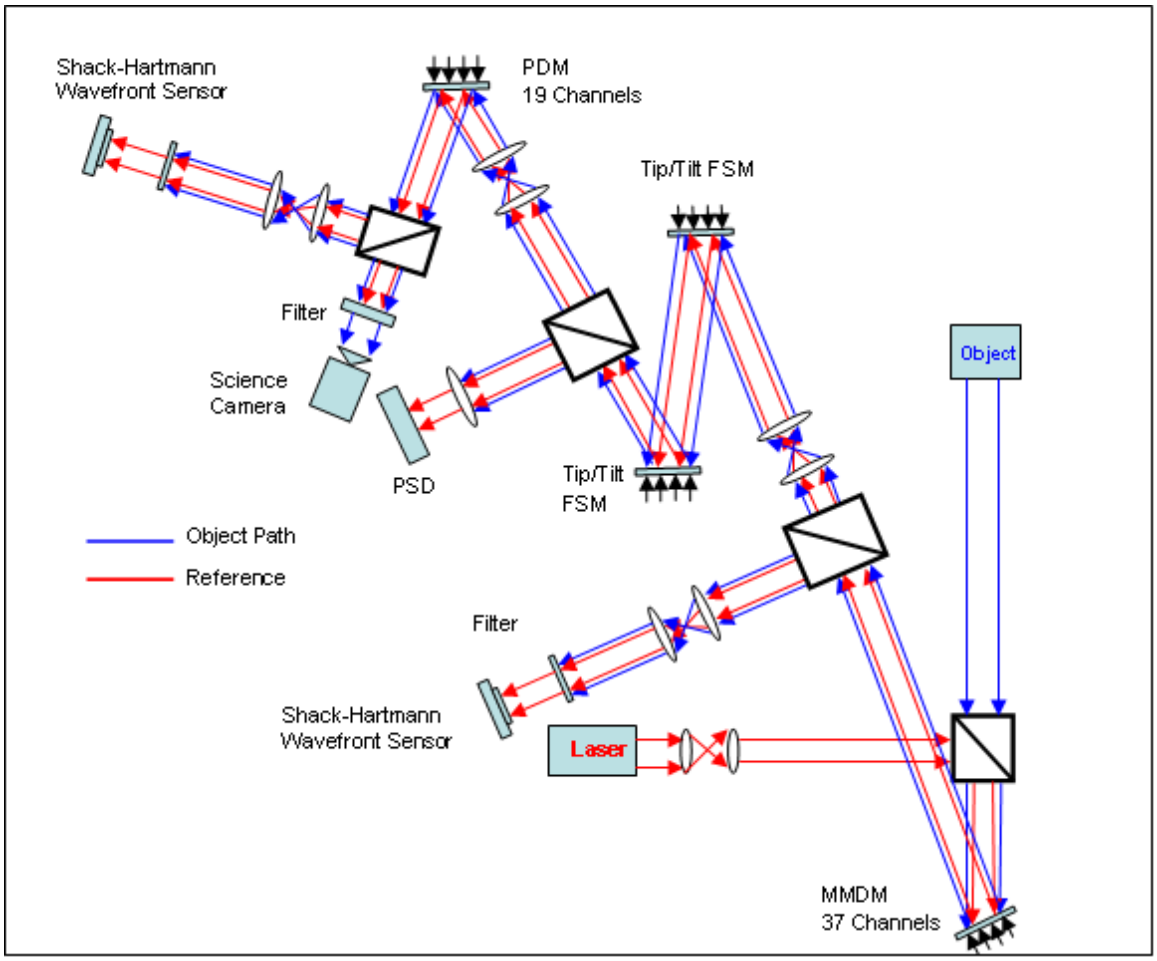

Figure 9 AO Testbed Picture.

Light from the reference laser beam and the object light are combined at the first beam splitter. This combined light is then reflected off a Micromachined Deformable Mirror (MMDM). A Shack-Hartmann wavefront sensor measures a portion of the reflected reference light source and the rest continues through the system. The Shack-Hartmann wavefront sensor sends its CMOS camera image to the control computer, which converts the CMOS image into a set of wavefront slopes. A control algorithm is used to determine the correction necessary to make the wavefront planar, and a set of

voltages is sent to the deformable mirror to implement the correction. This is the first closed loop control system on the testbed.

A filter in front of the Shack-Hartmann wavefront sensor removes the white object light prior to hitting the lenslet array. Therefore, any wavefront aberrations are measured on the reference beam, not the object light. There are two important assumptions of this setup. The first is that the same aberrations are present in the reference beam as the image beam. Second, correcting the reference beam will also correct the object light. It is possible that since the laser light is monochromatic while the object light contains all visible wavelengths, some of the optical elements on the table could cause chromatic aberrations in the object light that are not present in the laser beam. These differences are assumed to be negligible.

After the first closed loop wavefront correction process, the combined light beam next encounters two Fast Steering Mirrors (FSMs). Including just one FSM allows tip/tilt jitter aberrations to be removed. The presence of two FSMs allows the injection of a disturbance with the first FSM to simulate an on-board jitter, and the removal of the jitter with the second FSM. Of course, in their nominal configuration, when no commands are sent to the actuators on the FSMs, they behave as ordinary planar mirrors. The Position Sensing Detector (PSD) in the schematic is the wavefront sensor used to close the control loop with the second FSM.

The combined light beam next encounters a second deformable mirror, this one having piezoelectric actuators (PDM). Like the first DM, the light reflected off it is imaged by a Shack-Hartmann wavefront sensor and analyzed by a second control computer to determine the proper correction to be applied by the DM. This completes the final closed loop system on the testbed. Finally, the reference laser beam is filtered out and a science camera is able to take an image of the object light as seen in Figure 7.

2. Hardware

This section will give specifics on some of the AO testbed hardware. The control laws developed involve only the components in the first closed loop system; the MMDM and one Shack-Hartmann wavefront sensor. The other components did not have an active role in verifying the performance of the control laws.

a. Laser

The laser on the testbed is a red HeNe laser with a wavelength of 632.8 nm. It is manufactured by JDS Uniphase and the model number is 1137P.

b. Micromachined Deformable Mirror

The MMDM is manufactured by OKO Technologies of Delft, the Netherlands. The following information is taken from the user manual [19]. The aperture is 15 mm in diameter. Thirty-seven actuators are located under a 12 mm diameter of the membrane with 1.8 mm center-to-center spacing between actuators. A diagram is shown in Figure 10. The mirror itself is a silicon chip coated with a silicon nitride membrane. The numbering and two-dimensional positioning of the actuators is shown in Figure 11.

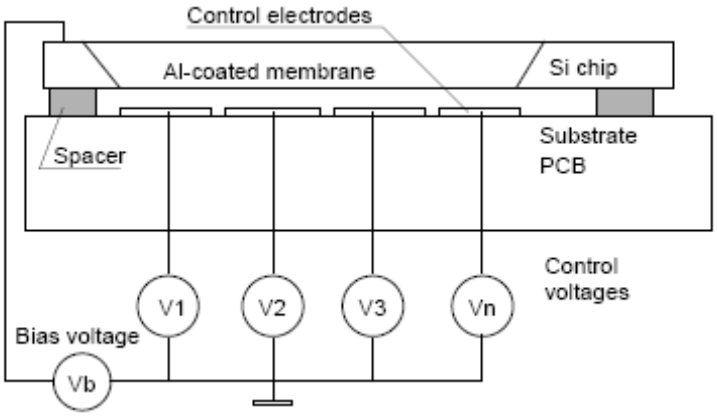

Figure 10 MMDM Schematic Section From [19].

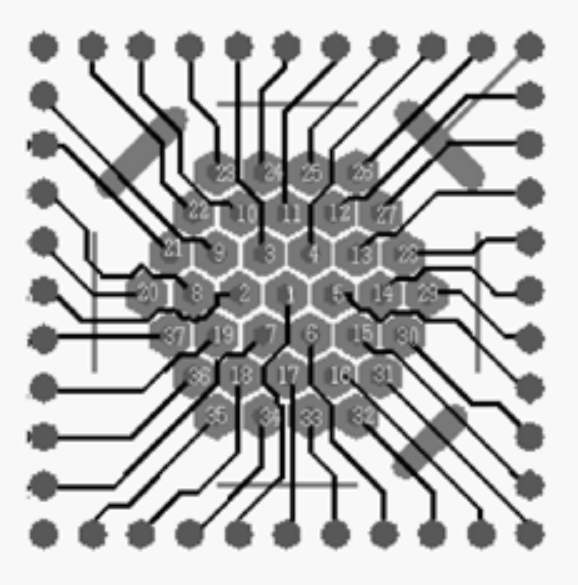

Figure 11 MMDM Actuator Locations and Positioning From [19].

c. Shack-Hartmann Wavefront Sensor

OKO Technologies [19] also provides the Shack-Hartmann wavefront sensor on the testbed. It is a ½-inch CMOS A601f camera manufactured by the German company Basler with a Hartmann lenslet mask from OKO installed. The sensor has 656 x 491 pixels and a frame rate of 30 frames per second. The lenslet mask has 127 lenslets laid out in a hexagonal array and coated with a fused silica coating. The aperture size is 3.5 mm and the subaperture of each lenslet is 100 μm. The appearance of the array is similar to that of one of the segments in the segmented space telescope model array shown in Figure 5, only with 127 lenslets vs. 61.

d. Control Computer

The control algorithms are implemented on a standard desktop PC and Matlab software. The computer is a Pentium D with a 2.8 GHz processor and 1.0 GB of RAM. The operating system is Windows XP version 2002, service pack 2. The Matlab version is R2007a. The Basler camera is connected via fire wire to the computer, and two PCI cards connect the computer to the MMDM. One card controls 19 actuators, the other, 18.

THIS PAGE INTENTIONALLY LEFT BLANK

III. ROBUST CONTROL

A. TRADITIONAL CONTROL APPROACH

The purpose of any control system is to provide stability and achieve certain performance objectives. For adaptive optics systems, classical control techniques have always been adequate. Their simpler design process and more intuitive nature make them the controller of choice for most applications. The following will give a brief overview of the traditional AO system control approach and identify the shortcomings that led to this research into more advanced control techniques.

Traditionally, the adaptive optic in large ground based AO systems is treated as a static system with no dynamics. In the case of a deformable mirror, it is assumed that the coupling between actuators is static. Classical control approaches neglect the dynamics associated with this coupling thereby simplifying the control process [3], [5]. Obviously, as the optics for space telescopes become lighter as discussed in Chapter I, and as more actuators are packed into a given area to provide higher spatial correction, this simplifying assumption becomes less realistic. For systems with a high degree of internal dynamics, instability can result from a controller designed from a static model.

At the basis of the control algorithm, the reconstruction, or influence matrix, relates the actuators with the aberrations in the wavefront. The reconstruction matrix is formed by starting with the mirror in a neutral position and then actuating or poking each actuator in turn while measuring the effect on the wavefront. For this reason, the reconstruction matrix is often referred to as the poke matrix. As an example, consider a deformable mirror with 10 actuators and a Shack-Hartmann wavefront sensor with 20 lenslets. Assume the neutral position of each actuator is represented by a 0, and it can be commanded to any value from -1 to +1. Actuator 1 is given full positive stroke and an image is taken with the Shack-Hartmann wavefront sensor. This measurement yields a vector of 40 measurements (20 *x* and 20 *y*.) Actuator 1 is reset to 0, and the process is repeated for actuator 2. The end result is a reconstruction matrix with dimensions of [40 x 10] where each column represents the *x* and *y* pixel displacements on the camera sensor

for each individual actuator. These x and y pixel displacements can be easily converted to x and y slopes by multiplying by the physical pixel width and dividing by the camera focal length.

This process creates a map of how an actuator position or command affects the wavefront, but it neglects the structural dynamics of the mirror. The mathematical expression of the reconstruction matrix, R, is given as

$$R = \begin{pmatrix} S_1^{x1} & \cdots & S_1^{xm} \\ \vdots & & \vdots \\ S_n^{x1} & \cdots & S_n^{xm} \\ S_1^{y1} & \cdots & S_1^{ym} \\ \vdots & & \vdots \\ S_n^{y1} & \cdots & S_n^{ym} \end{pmatrix} \tag{3.1}$$

where S is the slope in the x or y direction, n is the number of lenslets, and m is the number of actuators. The relationship between the actuator input vector, $\underline{u}$, and the slope measurement vector, $\underline{S}$, is given by

$$\underline{S} = R\underline{u} \tag{3.2}$$

Since the slope is the measured quantity, the pseudo-inverse of the reconstruction matrix is used to determine the control inputs. One possible control approach is to subtract the product of the inverted reconstruction matrix (found with a pseudo-inverse technique) and measured slope from the previous control input as shown in Equation (3.3). This will drive the control signal to a steady state value and the wavefront slope to zero, resulting in a planar wavefront.

$$\underline{u}_{new} = \underline{u}_{old} - R^{\dagger}\underline{S} \tag{3.3}$$

Variations on how the wavefront is determined from the slopes (e.g., modal or zonal) and variations on the feedback method (e.g., direct, indirect, iterative, etc.) can be employed to improve the performance for this traditional control law [3].

As stated before, the classical control approach ignores the structural dynamics of a system. Even if a more complex multi-input, multi-output control approach was used that accounted for dynamics and coupling between actuators, it would still need to

perform satisfactorily in the presence of external disturbances and unmodeled dynamics. These uncertainties give credence to the idea of designing robust controllers for AO systems.

B. JUSTIFICATION FOR ROBUST CONTROL

Robust control addresses the problem of designing a control system that yields a desired performance in the presence of model uncertainties and external disturbances. For the purposes of this research, the plant to be controlled is a state space model of the following form

$$G = \begin{cases} \dot{x} = Ax + Bu \\ y = Cx + Du \end{cases} \tag{3.4}$$

where x is the state, y is the measured output, and u is the control input. The robust control synthesis process augments the plant, G, into a modified system, P, with two input vectors and two output vectors. The process of constructing the modified plant, P, will be described later. The robust controller, K, is then designed for this augmented plant shown in Figure 12

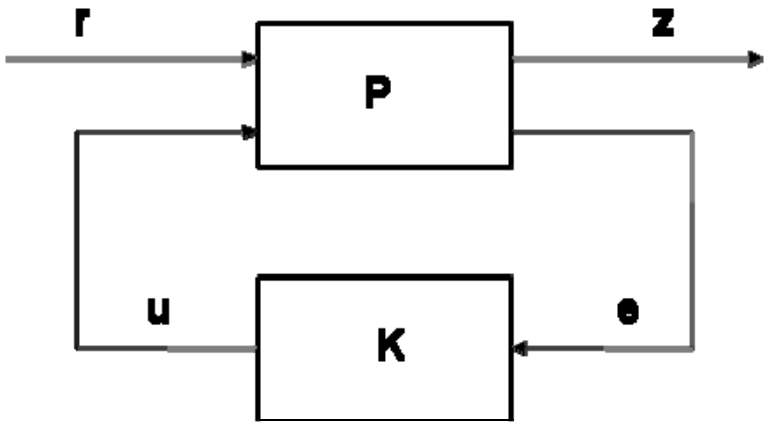

Figure 12 Standard Robust Control System.

where the plant, P, and controller, K, are both state space models, r is the external input (which contains a reference input, external disturbances, and noise), z is the performance measure, u is the control input, and e is the error between the reference input and measured output. For the specific case of the segmented space telescope model used for

this research, the state space plant model describes both the actuators and the Shack-Hartmann wavefront sensor outputs. The external inputs, *r*, are all zero. The reference input is usually zero for adaptive optics applications since a planar wavefront is desired; however, in some situations a non-zero reference input may be used if a particular aberration mode is desired. Since the error signal, *e*, is the difference between the measured output, *y*, and the reference, *r*, and the reference is zero, the error becomes simply the negative of the measured output. The control input, *u*, is a vector of actuator voltages. For this research the performance measure, *z*, is comprised of two components, the first is the error signal, *e*, and the second is the measured output, *y*. These two performance measures will be penalized or weighted differently for the controller synthesis process. This weighting process will be discussed shortly. The end goal then of the robust controller synthesis process is to minimize the ∞-norm of the operators from $r \to z$.

The overall goal of a robust controller is to provide stability for a system in the presence of uncertainty or unmodeled dynamics as discussed in Chapter I. Ideally, a robust controller will be able to handle these uncertainties better than other controllers such as classical PID controllers or optimal linear quadratic regulators. When speaking of robustness, there are two different performance criteria implied: the ability to handle uncertainty in the model, and the ability to reject disturbances and noise. What separates the robust control design process from a traditional control design process is that these uncertainties are explicitly accounted for in the design process to improve performance in the face of uncertainties that are poorly understood or modeled. The H_∞ robust control method minimizes the upper bound of the performance signal.

What follows are some of the mathematical foundations that form the backbone of robust control theory. Much of the material is general in nature and not specific to the research performed on the analytical segmented space telescope model. The topics include system norms, sensitivity and complimentary sensitivity functions, uncertainty modeling, and some of the tools necessary for the formulation of the appropriate augmented system matrix, *P*, to which the controller is synthesized. The application of these techniques to the analytical model will be covered in Chapter V.

C. MATHEMATICAL FOUNDATIONS

1. Norms

The basic premise of robust control involves minimizing a system norm. The type of norm is dependent on the type of robust controller being designed. A general overview of norms follows. From a conceptual point of view, a norm is nothing more than a measure of how large something is, such as the size of a vector. The general form of a vector norm in $\mathbb{C}^p$ as shown in [16] is given as

$$\|x\|_p := \left(\sum_{i=1}^{N} |x_i|^p \right)^{1/p}, \quad 1 \le p < \infty \tag{3.5}$$

where p takes on the value of the desired norm. The 1-norm and 2-norm (also known as the Euclidean norm) are common norms. In the case of robust control, a common norm, and the one used in this research, is the infinity-norm, given as

$$\|x\|_\infty := \max_{1 \le i \le n} |x_i| \tag{3.6}$$

The standard designation for this type of controller is H_∞, where the H refers to the Hardy space for stable systems.

For matrix operations, the induced norm becomes more useful, where the norm can alternately be thought of as a gain. Given the following simple transformation where A is the gain or amplification of the system

$$y = Ax \tag{3.7}$$

the induced matrix norm is given as

$$\|A\|_p = \max_{x \ne 0} \frac{\|Ax\|_p}{\|x\|_p} \tag{3.8}$$

2. Singular Values

Singular values are used extensively for robust control synthesis. Using a standard definition for linear algebra, singular values are the square root of the eigenvalues of a matrix times its adjoint (i.e., complex conjugate transpose) as shown by

$$\sigma_i = \sqrt{\lambda_i (A^* A)} \tag{3.9}$$

It can be shown that the largest gain for any input direction is equal to the maximum singular value, $\bar{\sigma}$, and that the smallest gain for any input is equal to the minimum singular value, $\underline{\sigma}$. The H_∞ norm can also be defined as the least upper bound on the maximum singular value. The H_∞ norm for a linear time invariant system, *G*, is given as

$$\|G\|_\infty \equiv \sup_\omega \bar{\sigma}\left(G(j\omega)\right) \tag{3.10}$$

For multi-input, multi-output systems, a plot of the maximum singular values is analogous to the Bode magnitude plot for single-input, single-output systems.

3. Small Gain Theorem

One of the most fundamental concepts for robust control is the small gain theorem, which follows from the above discussion of norms. For stability analysis, the small gain theorem replaces the traditional concepts of gain and phase margin. Consider the system in Figure 12 with uncertain elements Δ added as shown in Figure 13.

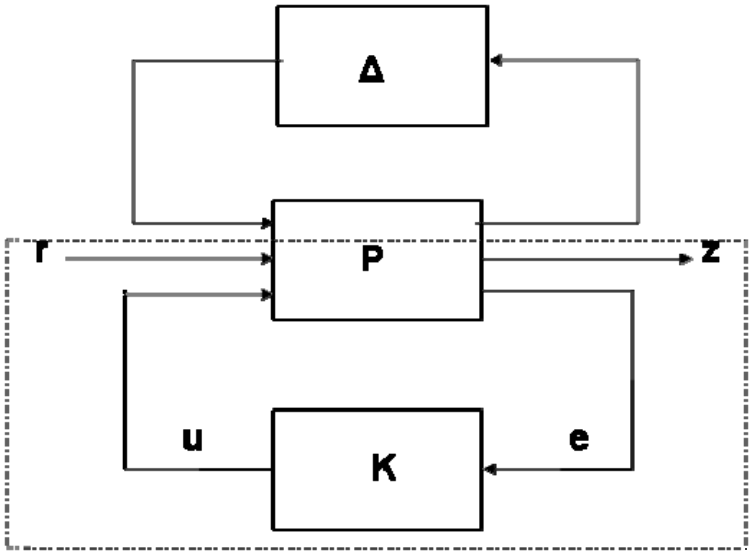

Figure 13 System with Uncertainty.

Let the region inside the dashed line, which is identical to the system in Figure 12, be represented as *M*. The small gain theorem requires than the gain (norm) of the uncertainty, Δ, multiplied by the gain of the system, *M,* must be less than 1 for the system to be robustly stable as shown by

$$\|\Delta\| * \|M\| < 1 \quad \forall \Delta \tag{3.11}$$

where the * represents a multiplication.

Another common form of the small gain theorem is given as

$$\|\Delta\|_\infty \leq 1/\gamma \;\; iff \;\; \|M\|_\infty < \gamma \tag{3.12}$$

where γ is a bound and $\gamma > 0$.

4. Sensitivity Functions

Two other necessary concepts for robust control design are the sensitivity function and the complementary sensitivity function. These functions allow the designer to shape the frequency response of the system in a manner similar to classical loopshaping techniques. The sensitivity function is important for shaping the response of lower frequencies, while the complimentary sensitivity function helps shape the high frequency response [20]. Mathematically, for a system consisting of a plant, *G*, and a controller ,*K*, with negative feedback, the sensitivity function, *S*, has the following form

$$S = (I + GK)^{-1} \tag{3.13}$$

From this, it follows that the complementary sensitivity function, *T*, has the following form

$$T = GK(I + GK)^{-1} \tag{3.14}$$

Due to their complimentary nature, the following is true

$$S + T = 1 \tag{3.15}$$

A control design process that incorporates loopshaping with both the sensitivity and complementary sensitivity functions is often referred to as a mixed-sensitivity problem [20]. In this instance, the sensitivity function influences the performance of the controller, and the complementary sensitivity function influences the stability of the system at higher frequencies. Figure 14 gives a representation of how loopshaping of the

sensitivity and complementary sensitivity functions can affect the controller / plant system, represented by L ($L = GK$) in the figure.

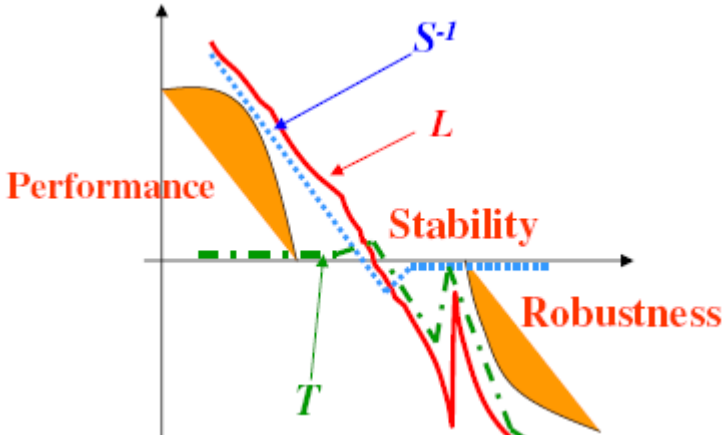

Figure 14 Robust Control Loopshaping From [20].

At low frequencies, the loop transfer function, L, is weighted to follow the inverse of the sensitivity function. The sensitivity function of the system describes how well the controller does at providing for disturbance rejection, tracking errors, and negating any plant parametric variations. Shaping the sensitivity function indirectly shapes the loop transfer function, and in some cases vice versa. At higher frequencies, the shape of the complementary sensitivity function describes the transient response and stability. The complementary sensitivity function is shaped by weighting functions in the same way as the sensitivity function.

5. Weighting Functions

At this point, it is necessary to introduce a set of weighting functions that will manipulate or shape the sensitivity and complementary sensitivity functions. The weighting functions can take whatever form is appropriate for the system, but for the purpose of this research, first order transfer functions are satisfactory. The first weighting function, introduced as W_1, is a penalty on the error and affects the lower frequencies and shape of the sensitivity function. A second weighting function, W_2, is a penalty on the control signal but is not used in this research. The final weighting function, W_3, is a penalty on the measured output and affects the complementary

sensitivity function and higher frequencies. Figure 15 shows a schematic of a nominal system with a plant, a controller, and weights W_1 and W_3. Note that the transfer functions shown in the figure merely represents a generic transfer function and not the actual weights used.

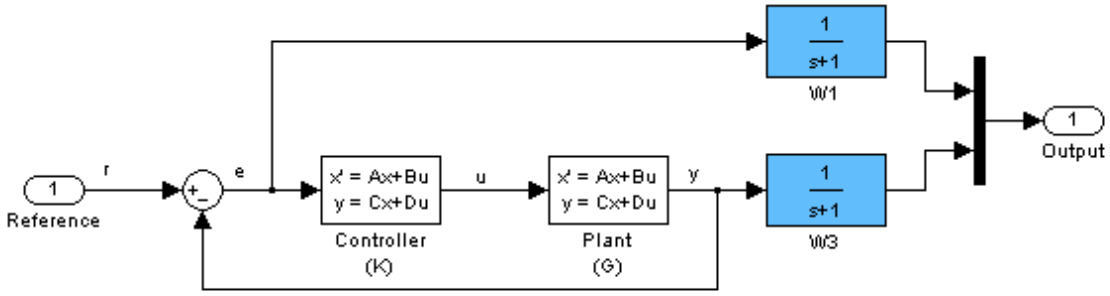

Figure 15 Schematic of System with Weighting Functions.

The weighted error and measured output signals together form the performance measure previously identified in Figure 12 as *z*. The error that is weighted by W_1 is minimized in order to achieve the desired performance by influencing the sensitivity function. The output that is weighted by W_3 is minimized in order to achieve stability in the presence of higher frequency disturbances by influencing the complementary sensitivity function. Satisfying both of these goals simultaneously may not be possible; thus an iterative approach to synthesizing the robust controller is used. If the weights selected are too restrictive on the design, a robust controller meeting the design requirements cannot be synthesized.

The closed loop system with weight W_1 is said to have robust performance if the following condition of the small gain theorem is met

$$|W_1| < |1 + GK| \quad \forall \omega \tag{3.16}$$

Similarly, when considering W_3 and the complementary sensitivity function, the system is robustly stable if the following condition is true

$$|W_3 GK| < |1 + GK| \quad \forall \omega \tag{3.17}$$

Combing equations (3.16) and (3.17), the system has both robust performance and stability if the following is true

$$\left\| |W_1 S| + |W_3 T| \right\|_\infty < 1 \tag{3.18}$$

Designs that employ a weight on both the sensitivity function and the complementary sensitivity function are referred to as weighted mixed sensitivity problems [20].

D. MODEL UNCERTAINTY

The main advantage of designing a robust controller over other simpler classical techniques is the ability to handle model uncertainties. While certain designs allow for wide latitude in handling uncertainties, it would be nearly impossible to design one controller for all possible uncertainties a system might encounter over its lifetime. Therefore, it is necessary to understand what kinds of uncertainty are likely, where they come from, and how to bound the uncertainties to simplify some of the design constraints. Uncertainty can be added to a system in two different ways, an additive fashion or a multiplicative fashion. The following two figures depict these two methods. Perturbations of these types can be added to any combination of inputs or outputs to the system.

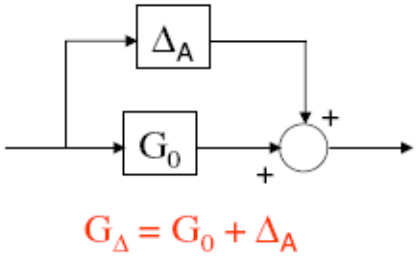

Figure 16 Additive Uncertainty From [20].

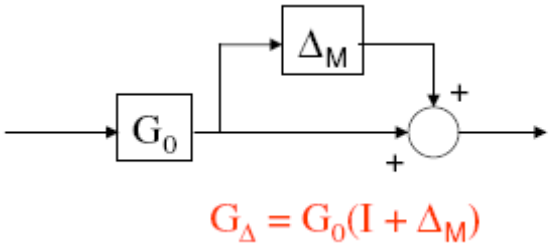

Figure 17 Multiplicative Uncertainty From [20].

The first consideration in defining the uncertainty to be added to a model is to define it as structured or unstructured. An unstructured uncertainty is a bounded perturbation that is included or added to the model, but where very little of the nature of the perturbation is known. For example, there is no transfer function that describes the general behavior of an unstructured uncertainty.

Structured uncertainties involve perturbations that are more understood than unstructured. In general, there are more constraints on the nature of a structured uncertainty than an unstructured uncertainty. Structured uncertainties can result from bounded variations in model parameters such as changes in the physical components of a system over time due to wear and tear. They also result from combinations of multiple uncertainties, or both additive and multiplicative perturbations. Figure 18 shows a diagram of typical structured and unstructured model uncertainties [17].

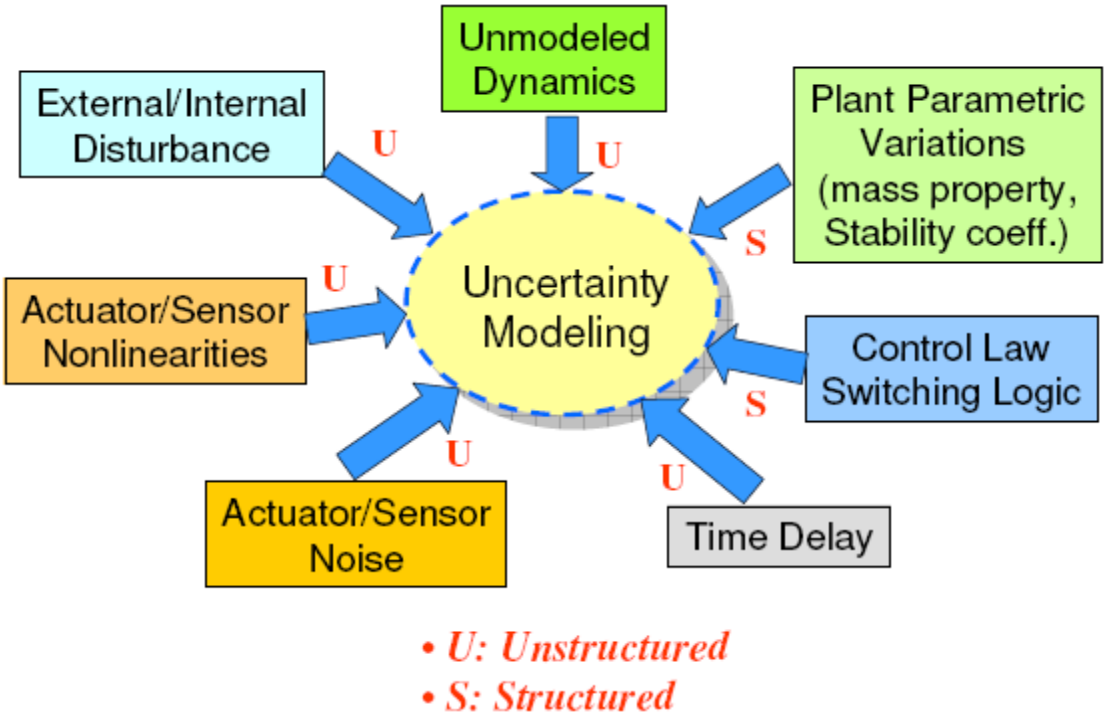

Figure 18 Structured and Unstructured Model Uncertainty Sources From [20].

In addition to helping shape the sensitivity and complementary sensitivity functions, the weighting functions also bound the system uncertainty [20]. For this reason, proper selection of the weighting functions becomes a crucial part of robust control design.

The segmented space telescope model used in this research does not contain any unstructured uncertainties. On the other hand, uncertainties on some of the physical parameters such as modal frequencies and damping are assumed. This affects the lower left quadrant where the squares of the natural frequencies are found in the following system *A* matrix

$$A = \left(\begin{array}{cc|cc} \ddots & & \ddots & \\ & 0 & & I \\ & \ddots & & \ddots \\ \hline \ddots & & \ddots & \\ & -\omega_n^2 & & -2\xi\omega_n \\ & \ddots & & \ddots \end{array}\right) \tag{3.19}$$

Uncertainty in the natural frequencies is a logical concern for a lightweight space telescope model such as this. Therefore, a percentage of uncertainty can be added to the natural frequencies to allow for explicit design of a robust controller based on an uncertain model.

E. CONTROLLER SYNTHESIS

The robust controllers designed for this research were based on minimizing the closed loop system ∞-norm. Other robust control synthesis methods exist such as those based on a 2-norm, but they will not be discussed here. The ∞-norm method used here is a direct method denoted as H_∞. This method designs a controller based on a nominal augmented plant as previously shown in Figure 12.

The H_∞ robust control design technique requires a properly constructed plant model to synthesize a robust controller. In order to achieve the robust performance and stability design objectives, the plant must be augmented with the appropriate weighting functions. A representation of this augmented nominal plant is shown in Figure 19.

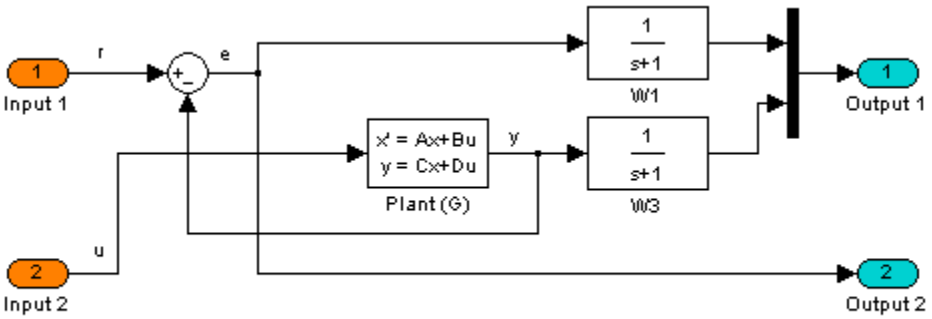

Figure 19 Augmented Nominal 2-Input, 2-Output Plant.

This augmented plant is often referred to as the 2-input, 2-output model. The two vector inputs to the augmented plant are the reference input and the control input, which the controller to be designed will provide. One of the vector outputs is the weighted error and weighted measured output signal combined, which is otherwise known as the performance measure. The other vector output is the error signal that is used as the input for the controller.

Once this 2-input, 2-output model has been constructed, the goal is to minimize the ∞-norm of the error signal to the command or disturbance input. A representation of how the weighting functions are included in the augmented model, P, is given as

$$P = \left(\begin{array}{c|c} W1 & -W1G \\ 0 & W3G \\ \hline I & -G \end{array}\right) \tag{3.20}$$

Since the original plant, G, was a state space model, P is also a state space model and can be partitioned as

$$P = \left(\begin{array}{c|cc} A & B_1 & B_2 \\ \hline C_1 & D_{11} & D_{12} \\ C_2 & D_{21} & D_{22} \end{array}\right) \tag{3.21}$$

where the A, B, C, and D matrices are the augmented state space matrices. The controllability and observability of the system can be determined using the submatrices

B_1, B_2, etc. As shown in [16], the following assumptions on the partitions of *P* are made before proceeding with the controller synthesis

- (A, B_1) is controllable
- (C_1, A) is observable
- (A, B_2) is stabilizable
- (C_2, A) is detectable
- $D_{12}^T \begin{pmatrix} C_1 & D_{12} \end{pmatrix} = \begin{pmatrix} 0 & I \end{pmatrix}$
- $\begin{pmatrix} B_1 \\ D_{12} \end{pmatrix} D_{21}^T = \begin{pmatrix} 0 \\ I \end{pmatrix}$

An admissible controller exists if and only if the following conditions are met:

- $H \in (Ric)$ and $X := Ric(H) > 0$
- $J \in (Ric)$ and $Y := Ric(J) > 0$
- $\rho(XY) < \gamma^2$

where *H* and *J* are the following Hamiltonian matrices

$$H := = \begin{pmatrix} A & \gamma^{-2} B_1 B_1^T - B_2 B_2^T \\ -C_1^T C_1 & -A^T \end{pmatrix} \tag{3.22}$$

$$J := \begin{pmatrix} A^T & \gamma^{-2} C_1^T C_1 - C_2^T C_2 \\ -B_1 B_1^T & -A \end{pmatrix} \tag{3.23}$$

γ is a performance bound with $\gamma > 0$, *Ric* is the solution to an algebraic Riccati equation of the form

$$A^T X + XA + XBX + C = 0 \tag{3.24}$$

and ρ is the spectral radius with

$$\rho(A) := \max_{1 \le i \le n} |\lambda_i| \tag{3.25}$$

The robust control design algorithm iterates on the value of γ between 0 and infinity with a bisection algorithm until such time as a solution to the Riccati equation

cannot be found. Once the specified tolerance threshold has been reached the iteration stops and the controller, K, can be computed from the following equations

$$K = \left(\begin{array}{c|cc} A_f & -ZL & ZB_2 \\ \hline M & 0 & I \\ -C_2 & I & 0 \end{array}\right) \tag{3.26}$$

where

$$M = -B_2^T X \tag{3.27}$$

$$L = -YC_2^T \tag{3.28}$$

$$Z = \left(I - \gamma^{-2} YX\right)^{-1} \tag{3.29}$$

$$A_f = A + \gamma^{-2} B_1 B_1^T X + B_2 M + ZLC_2 \tag{3.30}$$

Figure 20 shows the synthesized controller, K, attached to the augmented plant from Figure 19. Figure 20 is now identical to the original system presented in Figure 12.

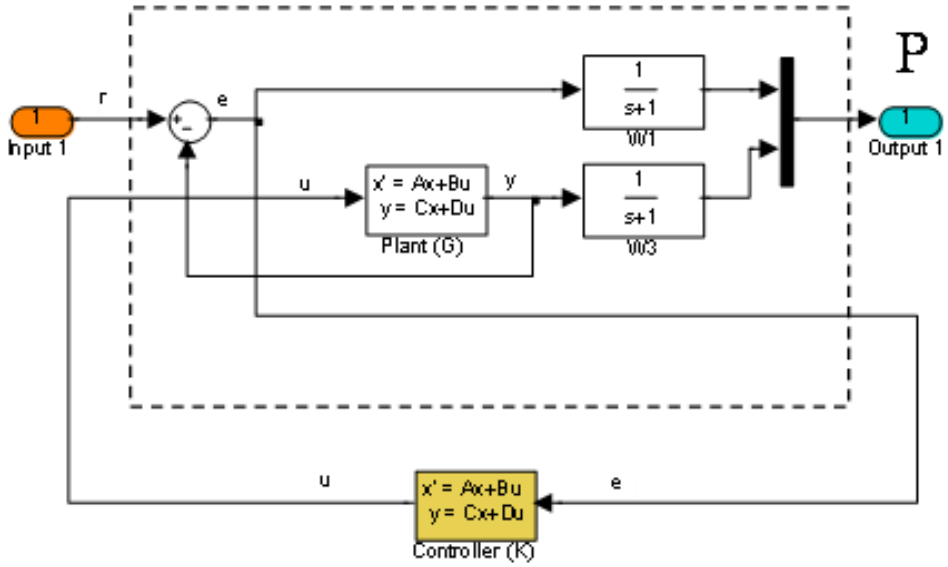

Figure 20 Augmented Plant and Controller.

The controller synthesis consists of designing the controller, K, such that the following cost function is minimized

$$\|T_{zr}\|_\infty < \gamma \tag{3.31}$$

where T is the closed loop transfer function. After this design process has generated the H_∞ controller, it can be implemented as a continuous system, or discretized prior to implementation. The application of these techniques to the segmented space telescope model will be discussed in Chapter V.

IV. MODEL REDUCTION TECHNIQUES

A. INPUT/OUTPUT REDUCTION

The robust controller synthesis process described in Chapter III can be rather computationally prohibitive. In the case of the analytical segmented space telescope model, the 332 states, 997 inputs, and 936 outputs are more than an average desktop computer can process. Therefore, some kind of model reduction is necessary. This chapter will present an innovative method developed to reduce the inputs and outputs as well as a standard method of state reduction.

1. Singular Value Decomposition

The principle behind the reduction method developed is the projection of a vector into a subspace. In this case, a large vector of input values is projected into a vector of many fewer values. If the projection is chosen carefully, then the important or significant values of the original vector are preserved so that when the reduced vector is expanded back to the original number of values, it is still representative. The Singular Value Decomposition (SVD) is one such technique that, by its very nature, preserves the significant values.

In general, the SVD has the following form

$$SVD(H) = U\Sigma V^T \tag{4.1}$$

where H, U, Σ, and V are all matrices, and Σ is a diagonal matrix with the singular values arranged in decreasing size. The matrices U and V are also ordered such that the vector associated with the largest singular value is in column one and so on. A plot of all the singular values helps to identify how many singular values have a sufficient impact on the final system so that a logical place to truncate the singular value matrix can be found. For example, if there are 40 total singular values, but the last 25 are significantly smaller than the first 15, those last 25 values can be truncated and the most important aspects of the original system are still preserved. Since the column vectors of the U and V matrices are also rank ordered into decreasing importance, only the first 15 column vectors of those matrices will be retained. As will be shown in Chapter V, when H is

defined to be the transfer function of the inputs to the outputs for the analytical space telescope model, the large number of inputs or outputs of the original system can be projected into the column vectors of the truncated *U* and *V* matrices. The inputs are projected via the *V* matrix and the outputs are projected via the *U* matrix.

Once a controller has been synthesized for this reduced input/output model, the controller outputs can be projected back into the total number of original plant inputs through the truncated *V* matrix. Similarly, the original plant outputs are projected into the truncated *U* matrix so that they may be inputs for the reduced controller.

2. Zernike Polynomials

An innovative approach developed in this dissertation is the use of Zernike polynomials for model output reduction. Zernike polynomials are orthogonal and normal about a unit circle, making them especially applicable to optical applications where the optical components have circular apertures. Their orthogonal and normal nature as described in [21] is shown by

$$\int_0^1 R_n^m(\rho) R_{n'}^m(\rho) \rho d\rho = \frac{1}{2(n+1)} \delta_{nn'} \tag{4.2}$$

where R_n^m is the radial polynomial and δ is the Kronecker delta. It is worth noting, however, that Zernike polynomials are but one of an infinite number of polynomial sets that are normal about a unit circle. Furthermore, variations on the Zernike polynomials exist depending on their particular application and usage. Derivations of the standard form of Zernike polynomials can be found in [22], [23]. A slightly modified form of Zernike polynomials known as the fringe Zernikes was developed at the University of Arizona and is used for this research [24]. The main difference is that the fringe Zernikes have been normalized to unity magnitude at the edge of the pupil. The expansion series of the fringe Zernike polynomials is given by

$$Z_n^m(\rho,\theta) = R_n^m(\rho) e^{im\theta} \tag{4.3}$$

where

$$R_n^m(\rho) = \sum_{s=0}^{n-m} (-1)^s \frac{(2n-m-s)!}{s!(n-s)!(n-m-s)!} \rho^{2(n-m-s)} \tag{4.4}$$